Low Voltage PV Interface to a High Voltage Input Source with Modified RVMR

Sathishkumar RAMASAMY[1], Deepamangai PALANIVEL[1], Subramanian P. MANOHARAN[2]
[1]*SRM TRP Engineering College, Trichy, Tamilnadu, India-621 105*
[2]*Thiagarajar College of Engineering, Madurai, Tamilnadu, India-625 015*
rskgct@gmail.com

***Abstract*—In this work PV fed Modified Resonant Voltage Multiplier Rectifier (RVMR) has been proposed for the hybrid renewable energy system. PV source energy is maximized in the modified RVMR scheme by applying the perturb and observe (P&O) based MPPT method. To incorporate modified RVMR for PV grid-connected systems and observe the improvement in dynamic response and voltage gain. In the proposed work, voltage gain and efficiency are analyzed and evaluated in the MATLAB/SIMULINK environment.**

***Index Terms*—converters, maximum power point trackers, photovoltaic cells, perturb and observe method, resonant converters.**

I. Introduction

Many modifications have been applied to the conventional boost converters for high-gain converter design. Those modifications are required to obtain adequate voltage gain and efficiency. Numerous reforms are being done to form a step-up high gain conversion for improving the voltage gain ratio. These can be categorized as isolated, non-isolated, and mixed-mode systems. Interleaving structures are one of the most utilized conversion topologies for achieving a high gain ratio. They have a dual conversion stage that suits the higher power conversion with a simpler phase shift control. There are various configurations of the step-up structures found in the literature and they utilize the interleaved manner to obtain higher gain with efficiency. The converters are being modified from the traditional boost converter for obtaining a higher voltage step gain by the addition of transformers and voltage multipliers [1].

A coupled inductor is used to boost the step-up gain of a boost flyback converter. This is a simple method for increasing the step-up gain. This converter has a leakage current at the load side since it resembles the active clamped flyback converter [2-3]. To raise the voltage, an interleaved boost converter with a voltage-lifting capacitor is used. Interleaved technology with a voltage lifting scheme is used in this approach. The voltage-lift capacitor provides additional voltage gain, and this, in turn, reduces the input current ripple. For PFC and high-power applications, it is an excellent choice. As time went on, a new step-up converter was proposed that combines the best features of all three converters. Voltage lifting and step-up gain with a minimum duty ratio control are among the advantages of both. Using a voltage-lift capacitor, coupled inductors can have a greater turn ratio, increasing the voltage gain ratio [4-6]. With low input ripple current and low conduction losses, this converter is suitable for high-power applications. The output terminal receives the energy from leakage. The main switch is protected from large voltage spikes. There is a significant difference in the main switch voltage stress and output voltage stress in the converter. A voltage multiplier module was proposed by [7-9] that interleaves high-step-up converters with voltage multipliers. Two coupled inductors and two switched capacitors make up the voltage multiplier module. The modified boost flyback forward interleaved configuration is incorporated between two conventional interleaved boost converters. Flyback conversion occurs when the switch on one phase is turned off, while forward conversion occurs when the switch on the other phase is turned off.

There is a series and parallel connection between the primary and secondary windings of the coupled inductors with N_p and N_s turns to reduce input current ripple. There are no differences in turn ratios between the coupled inductors. Power switches' duty cycles will be 180° out of phase if the converter runs in Continuous Conduction Mode (CCM). There are more duty cycles than zero in this case. It is later integrated with an interleaved boost converter and a voltage multiplier module, which is comprised of switchable capacitors and inductors. It is possible to increase the step-up gain by using coupled inductors and switched capacitors. Switching one of the switches will release energy from the magnetizing inductor into three separate paths. When diodes are turned off, the current through them is reduced to zero before the diodes are turned on, thus reducing conduction losses. Diode reverse recovery losses will be reduced by this. It was recently reported by [10] that they have developed a high-step-up DC-DC converter that has been coupled with an inductor and voltage doubler. In this converter, low voltage stress is applied to the power switches while achieving an appropriate duty ratio. In addition, the coupled inductor's leakage inductor can be used to recycle energy back to the output. According to [11], fuel cells can convert DC energy into DC energy when they are run with high step-up DC-DC converters. In order to achieve high step-up voltage gain, the proposed converter makes use of a multi-winding coupled inductor and a voltage doubler. Energy stored in a leakage inductor is reclaimed by a clamping voltage on an active switch. Because of this, the voltage stress on the active switch is reduced and the conversion efficiency is increased. Low-input-voltage fuel cell power conversion can use the proposed high step-up converter. Hsieh et al. have proposed a new high-step-up DC-DC converter for a distributed generation system [12-15]. Two capacitors, two diodes, and a single coupled inductor make up this circuit. The coupled

Digital Object Identifier 10.4316/AECE.2022.04003

inductor charges and discharges two capacitors in series. It is possible to achieve a high gain voltage step-up with an appropriate duty ratio. A passive clamp circuit reduces the voltage stresses on the main switch and output diode. This is why it is recommended to use the main switch with a low resistance R. Diode reverse-recovery issues are alleviated, and the efficiency can be increased even further. A new interleaved high step-up converter is created by combining the WCCI concept with voltage multiplier cells [16-17]. The WCCIs have prolonged the voltage gain and reduced switch voltage stress. As a result of the circuit's voltage multiplier cells, low-voltage MOSFETs with high performance can be used in step-up and output voltage applications with low peak current ripple. WCCIs' leakage inductance has also reduced reverse-recovery losses, lessening the output diode's reverse-recovery problem. To progress the efficiency and decrease switching losses, power switches implement Zero Current Switching (ZCS) turn-on.

With the incorporation of transformers, they have created a new way to integrate low-voltage inputs into traditional step-up converter configurations, which were previously modified. The transformers are the primary focus of the design, and as a result, the issues of efficiency and isolation between the source and the load must be taken into consideration [18-20]. In general, the output voltage of a photovoltaic system is low and remains constant over time. The DC voltage rises when the panels are linked together in a series. However, the voltage imbalance at the module level is caused by the cascading of panels. Due to the varying output of solar panels, they must be used as frequently as possible. The cascading of panels can be enhanced with high-gain converters. The converters used for high-gain conversion should have high voltage gain ratios and excellent efficiency. Recently, DC-DC converters with high static gains have become one of the most popular topics of research because of the growing demand for low-voltage systems, such as those powered by renewable energy or batteries. Static high-gain, high-efficiency DC-DC converters are employed in the proposed work for better power conversion. This aids in obtaining the desired result while also integrating low-voltage input sources into the grid. Step-up Non-isolated boost converters, DC-DC converters are the most common type. Due to its relatively high output voltage and duty cycle of 0.8, this device can generally perform well in both dynamic as well as static conditions. For significant voltage gains, boost converters need large adjustments of duty ratios in addition to their inherent efficiency. It's a lot of stress on the boost switch when the duty cycle is high. To maximize efficiency, lower duty cycles are required, while parasitic resistive components limit voltage gain. There is a concern about reverse recovery because diodes conduct only briefly. The efficiency of the converter degrades with increasing input current and output voltage [21-24].

Figure 1 depicts a typical PV-based renewable energy system. A converter is considered if its static gain (q) is equal to or greater than 10. This work is intended to increase the static gain and improve the gain equal to or greater than 10. For improving efficiency and high power results various techniques have been utilized, here a non-isolated structure is applied.

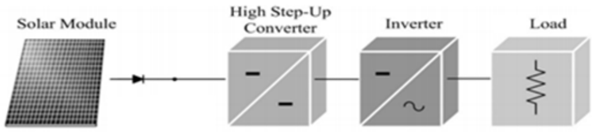

Figure 1. Typical PV-based renewable energy conversion system

Due to element resistances or leakage inductance, traditional step-up converters such as the boost converter and flyback converter cannot accomplish a high step-up conversion with good efficiency. Furthermore, traditional single-switch step-up converters are inadequate for high-power applications. These converters have a lot of voltage pressures. As a result, they are inappropriate for use in high-load applications with substantial input current ripple, which increases conduction losses.

II. Resonant Voltage Multiplier Rectifier and Modified Isolated Resonant Converter Operation

In isolated converters, transformer-based isolation is crucial to their efficiency. This is why high-step-up converters with galvanic isolation are preferred. Without transformers, it is impossible to calculate the isolation component. In order to provide the most power, the transformer must be operating at its optimum resonant state at all times. In isolated converters, transformer-based isolation is crucial to their efficiency. This is why high-step-up converters with galvanic isolation are preferred. The higher harmonic voltages are eliminated by the resonant network circuit. Zero Voltage Switching (ZVS) or zero current switchings (ZCS) is possible because of the resonant quality of the input current (ZCS) [25]. Thus, switching losses can be significantly reduced, and much higher switching frequencies can be attained. Passive equipment can be made smaller while power density is increased. A boost converter that operates in boost mode may have a higher conversion efficacy and voltage choice than an isolated Boost converter when it comes to efficiency and voltage range. To achieve maximum efficiency at the typical input voltage using a resonant Boost converter, it is not necessary to compromise efficiency at the highest or the lowest possible input voltages. All of this points to a successful implementation of high-step-up conversions using resonant converters. An improved converter is presented here that features high RVMR, constant frequency switching, and secondary side phase shift control.

III. Resonant Voltage-Multiplier Rectifier

Figure 2 shows the different structures of RVMR. The C_{r1} and C_{r2} are capacitors used in the designing of resonant tanks [26]. Also, four diodes are used in this circuit 1 and 3 act as output diodes, 2 and 4 diodes are regenerative diodes, and S1 and S2 are used to design the resonant tank with help of a high-frequency transformer (T). The N-type and P-type are shown in Fig. 2(a), whereas in the P-Type RVMR, the two switches are connected with the positive potential of the functioning principles of the two RVMRs are identical as illustrated in Fig. 2.

Unlike standard types, the RVMR's resonant tank always runs at the resonant frequency defined by Equation (1).

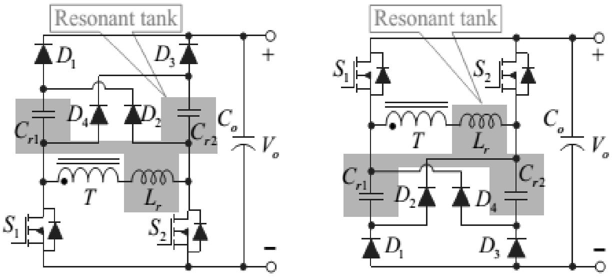

(a) (b)

Figure 2. Conventional resonant voltage multiplier rectifiers: (a) N-Type, (b) P-Type

$$f_r = \frac{\omega_r}{2\pi} = \frac{1}{2\pi\sqrt{L_r(C_{r1}+C_{r2})}} \tag{1}$$

As discussed earlier, the resonant tank will act as a boost inductor while turning on the RVMR. In the reverse case, after switching off the RVMR power regulation is occurred. So, owing to this operation high-frequency voltage is created on the primary side, i.e., the voltage-fed full-bridge circuit depicted in Fig. 3.

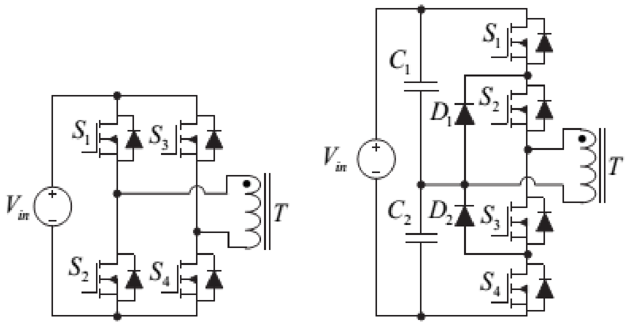

(a) (b)

Figure 3. Primary-side circuit: (a) Full bridge and (b) Three-level

The resonant circuit was designed using the primary of Lm and secondary of L_r in the ratio of 1:n with the help of Switches and diodes this was shown in Fig. 4. The voltage source used here is V_{in}, and the input voltage is amplified with help of a high-frequency transformer is n times, which was taken from the output source V_o which also acted as the load for the circuit.

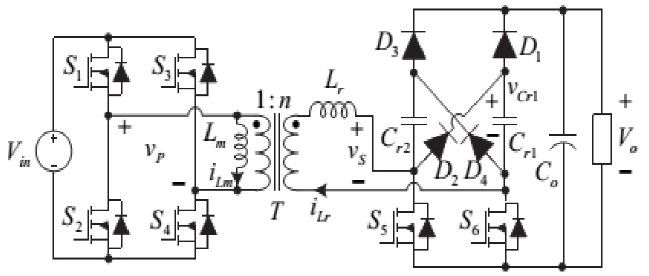

Figure 4. A modified full-bridge resonant converter based on the N-type RVMR

IV. MPPT Control of the Proposed Converter

Photovoltaic (PV) cells are used to convert sunlight into electrical energy. PV energy generated from the sun depends on the temperature and light illumination. In the proper irradiance and temperature, it gives good current-voltage waveforms, it is known as maximum power. To ensure maximum power, we need to introduce an algorithm called Maximum Power Point Tracking (MPPT). After employing the MPPT we can extract maximum power at every instant in the PV array.

The PV panels are subjected to environmental variations; In order to maintain maximum power tracing, the duty ratio of the converter is varied as PV panels are installed on the front side of the full-bridge controller. The maximum power to be extracted from the PV panels is done by altering the duty ratios of the full-bridge converters which are triggered with an alternative duty control.

The traditional P&O system is employed to abstract the maximum power. The P&O controller requires the voltage input and the solar irradiance along with the current. The input power and the output power are related to the converter to identify the power change. The method differentiates the change in the power fluctuations caused by the cyclic power variations. The change in voltage and power are compared by the P&O controller and then the perturbation direction is determined. When the PV panel operates in the MPP region the duty ratio is regulated. But instead, when PV panels are under non-MPP zones the deviations of the period size are varied in a larger magnitude.

V. Implementation of Modified RVMR for PV Integration

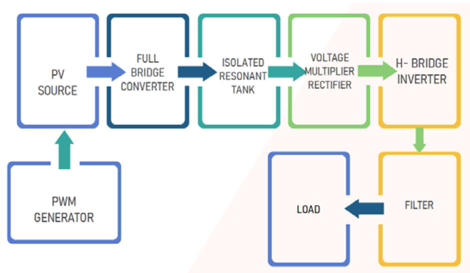

Figure 5. Block diagram of modified RVMR for PV integration

Thus, the controller always regulates the photovoltaic panel to extract its maximum power point under any condition. The block diagram of the modified RVMR for PV integration is shown in Fig. 5.

The modified RVMR for PV integration input voltage range of 40 V to 60 V has been taken into consideration. For this model, output has been taken in the range of 400 V with load consideration of 400 W and switching frequency in the range of 100 kHz. While designing these, L_r and C_r are the main factors for the resonant tank and output power which was obtained from Equations (2) and (3). The maximum ripple voltage is lesser than the inductor value.

$$C_r > \frac{P_0 T_s}{2V_0^2} \tag{2}$$

By substituting V_o=400 V, P_o=400 W, and T_S=10 µs, C_r>12.5 nF is obtained. Resonant inductor L_r should satisfy Equation (3):

$$L_r > \frac{V_0^2}{2\omega_r^2 P_0 T_s} \tag{3}$$

By substituting the parameters into Equation (3), L_r<101 µH is obtained. But in practical cases, S_5, S_6, and diodes D_1 and D_4, the voltage stresses on these devices will be ($0.5V_o+\Delta V_{Cr}$). The higher value of C_r will increase the size and volume of the resonant capacitance. In a practical case, two 22 nF capacitors were used to design the resonant capacitors. From Equation (2), the peak voltages of S_5, S_6, and D_1, D_4 are about 414 V and 400 V. The resonant inductor Lr should be 57.4 µH and the input voltage is 50 V after substituting in equation 1. By substituting the above values the transformer turns ratio (n) is carefully chosen as 4 considering V_{in}=50 V. From the primary side switches, the magnetizing inductance L_m output capacitance C_o≈1 nF of the transformer is selected with the help of ZVS. Meanwhile, the dead-time TDT is set to 70ns and then, the calculated result is L_m<52 µH.

From the consideration of secondary-side switches and diodes, 400 V rated can be used for D_1 and D_4 because, the peak voltage on the two diodes is about 414 V, whereas 600 V rated diode is used for D_2 and D_4. After applying the above design parameters the voltage stress has been on the two diodes is 400 V.

VI. Full-bridge LLC Resonant Converter Design

A two-carrier modulation technique is used to control the converter's operation. Full-bridge LLC resonant converter block diagram is depicted in Fig. 6. Phase shift angles can be determined from the PI regulator, which has two carrier signals. dS is in the secondary side switches because the controlled voltage V_{ctrl} is greater than V_{m1}, which is the output of the secondary side switches phase shaft modulator. Fig. 6 shows a typical resonant converter. Since soft-switching devices can be used to implement both the LLC converter and the existing converter, only the conduction losses are examined in this study. The voltage conversion ratio must be maximized by decreasing LLC resonant converter magnetizing inductance, L_m, because the circulating current introduced by L_m is significantly greater than that suggested. Primary-side switches, transformer winding, resonant inductor/capacitor, and resonant inductor/capacitor are subjected to greater current stresses and conduction losses in the LLC resonant converter than those in the proposed converter.

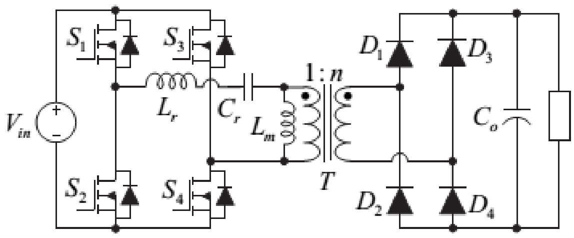

Figure 6. Full-bridge LLC resonant converter

However, the conduction losses of the rectifier diodes are lower in the LLC resonant converter because there are only two switches in the proposed RVMR, as opposed to four in the LLC resonant converter. The secondary-side current is significantly reduced in the current converter due to the higher output voltage.

As a result, there is less strain on the rectifying diodes of the LLC resonant converter and its two top diodes, D_1 and D_4, as well as the two switches. Reduced conduction losses and improved switching performance of low voltage-rated diodes and switches can then be used to reduce the amount of power lost. A DC-DC converter model was built to test the proposed converter's performance, and the secondary control stage was designed with a single source. Table I shows the results of a simulation model with a working prototype that tested the proposed converter's functionality. All of the converter's critical functions are put through their paces in a variety of conditions.

TABLE I. System Constraints of RVMR Circuit

Parameters	**Values**
Input voltage	40V-60V
Output	400V/400W
Switches S1-S6	MOSFETs
Inductor	56µH
Capacitor	22nF
Mutual Inductance	45µH
Turns ratio n	4:1
Diodes D1 to D4	Schottky Diodes

VII. Results and Discussion

When V_{in} is 50 V and V_{out} is 380 V, it does a boost as in Fig. 7. There are two switches on the primary side: S_1 and S_4. They both work 50 percent of the time, and S_2 and S_3 work 30 percent of the time. The secondary side switches work about half the time.

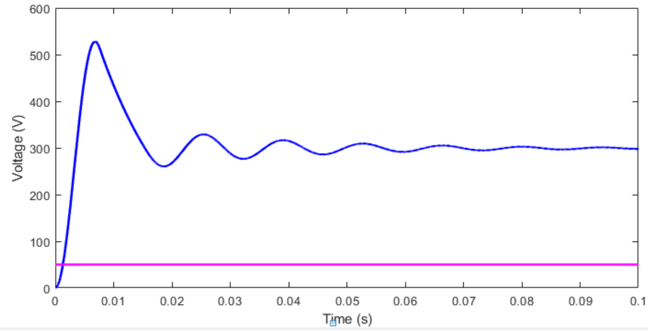

Figure 7. The output of the Boost mode changes when it is turned on.

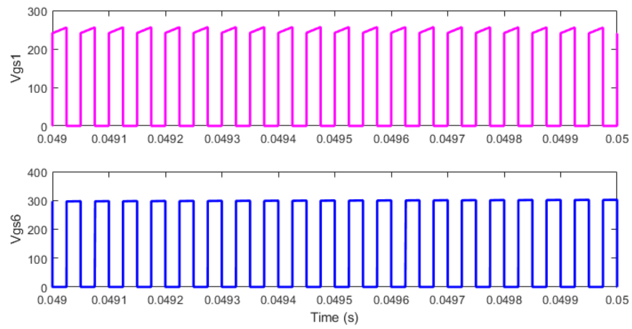

Figure 8. Waveforms of the boost mode

The resonant inductor, resonant capacitor, and driving voltages of S_1 and S_6 in the boost mode are shown in Fig. 8 and Fig. 9, which show the steady-state waveforms at the same time.

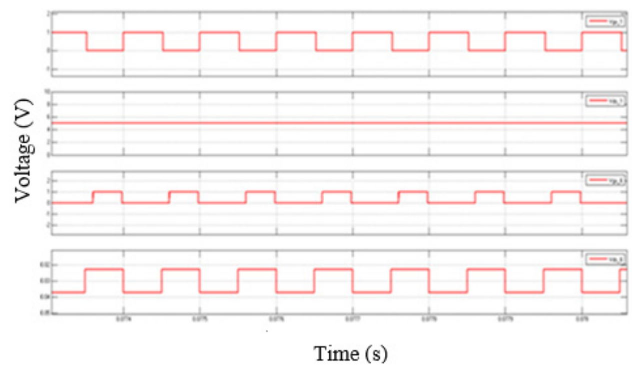

Figure 9. The soft switching waveforms of the switches S1 and S6

In this example, it can be observed that the driving signals of S_1 and v_{gs1} are delayed in comparison to the driving signals of S_6 and v_{gs6}, which indicates that $d_{\varphi P}<1$ has been achieved and the converter is operating in boost mode.

The soft switching patterns of the primary side S_1 and secondary side S_6 are shown in Fig. 9. These patterns work with the static zero voltage switching pattern, which increases the efficiency of the primary conversion when the secondary reaches zero.

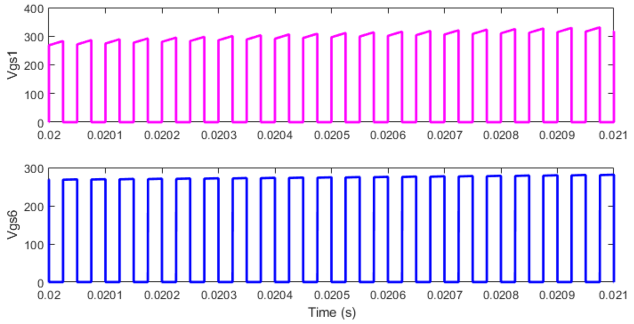

Figure 10. Resonant state waveform patterns

When the converter is in boost mode, the converter displays steady-state waveforms and voltages for a resonant inductor and capacitor.

As a result, the driving signals for S_6, V_{gs6}, and V_{gs1} are all behind the driving signals for S_1, which means that d_S>0. D_S>0 can be seen in the converter because $_{S6}$ and V_{gs6} are lagging behind S_1 and V_{gs1} in terms of driving signals. S_6 and V_{gs6} signals are behind schedule when compared to S_1 and V_{gs1} riding signals, which indicates that d_S>zero occurs inside the converter as shown in Fig. 10.

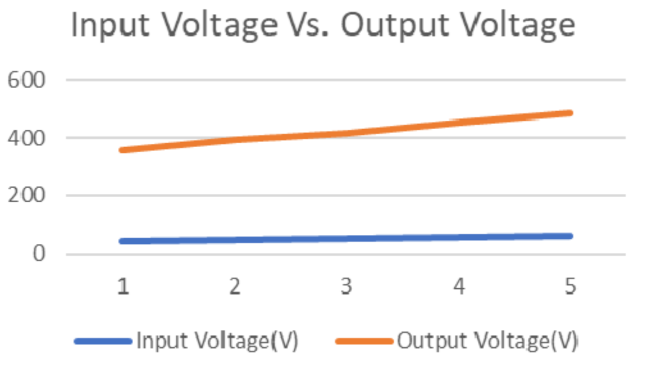

Figure 11. Input voltage and output voltage

A duty ratio control is depicted in Fig. 11 by displaying the input and output voltages. Using the secondary aspect voltage control, it is possible to maintain a constant voltage by increasing the voltage in the entrance aspect, much like the output voltage does.

In Fig. 12, where the efficiency curves are shown, more than 96 % efficiency was found for a wide range of voltages and loads. G=1 is the normalized voltage gain for high performance under 50 V input voltage.

When the voltage advantage G is greater than 1, the converter's performance suffers in the same way as a conventional buck-boost converter.

The converter's excessive light-load efficiency is demonstrated by the fact that it operates at 96 % efficiency even when the output load is only 15 % as shown in Fig. 12. The input and output voltages are 50 V and 300 V, respectively, under constant irradiation shown in Fig. 13.

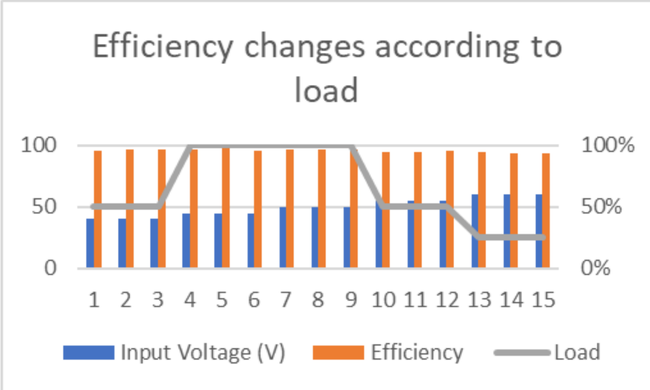

Figure 12. Input voltage and efficiency

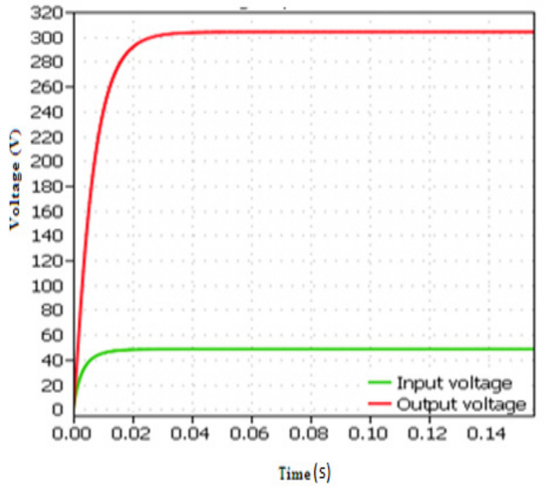

Figure 13. Input and Output voltage pattern with constant irradiance

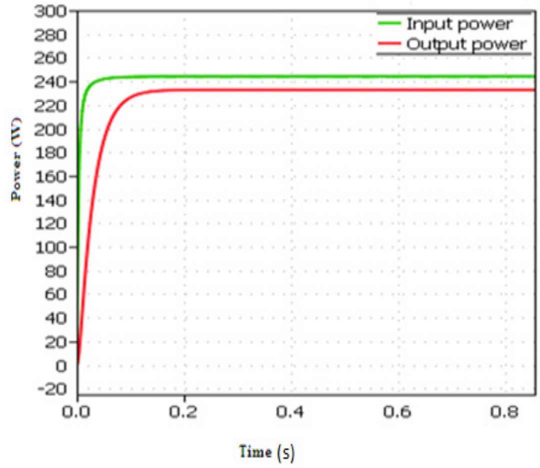

Figure 14. Input and the output power patterns of the P&O tracking scheme with constant irradiance

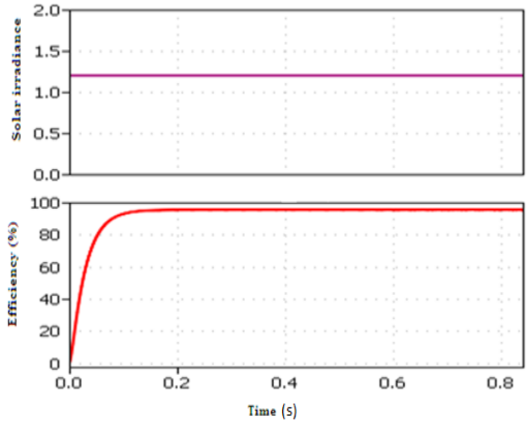

Figure 15. Tracking efficiency of the MPP scheme

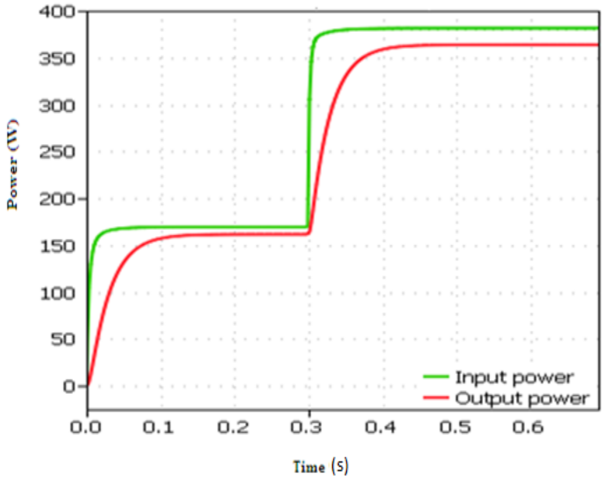

Figure 16. Input and the output power patterns of the MPP tracking scheme with step variations

The dissipated power and output power of the proposed control circuit are shown in Fig. 14, which is closer to the uniform radiation power supply.

The efficiency of the constant radiation converter is shown in Fig. 15, the maximum power is set to about 95% and the tracker manages the maximum efficiency without fluctuation in a minimum time. of 0.2 seconds.

Figure 16 shows that the gradual change in power indicates the efficiency of the proposed algorithm. The proposed technique shows a better control speed compared to the existing tracker standing for about 0.2 seconds, and when changing the step, the tracker adjusts the efficiency near the maximum point, adjusting much faster.

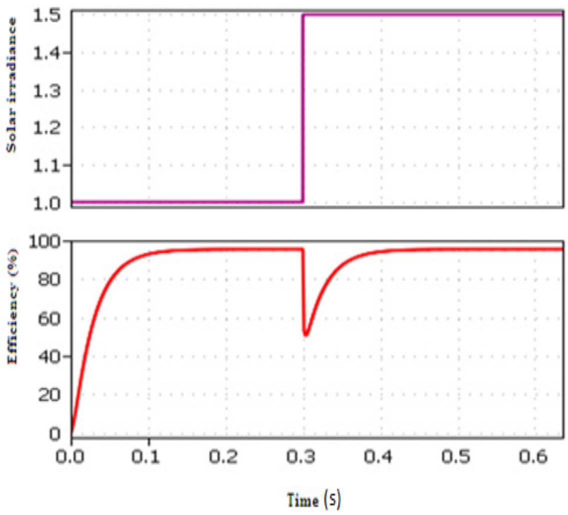

Figure 17. Solar irradiance vs efficiency under step change irradiance

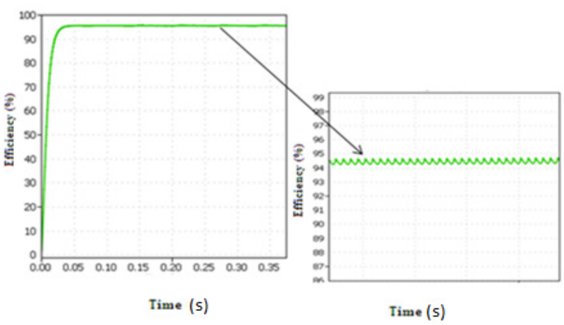

Figure 18. P&O under constant irradiance

Figure 17 shows a schematic diagram of the change in sunlight with a periodic efficiency of about 0.15 s, and the efficiency without high-level oscillations under the change in radiation is set at 0.1 s. P&O MPPT is shown in Fig. 18 and shows that the converter operates at the high efficiency of 94 % in a minimum installation time.

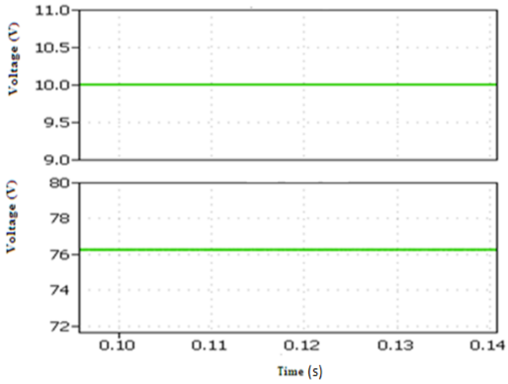

Figure 19. When the input voltage is 10V, the RVMR output voltage will be 76

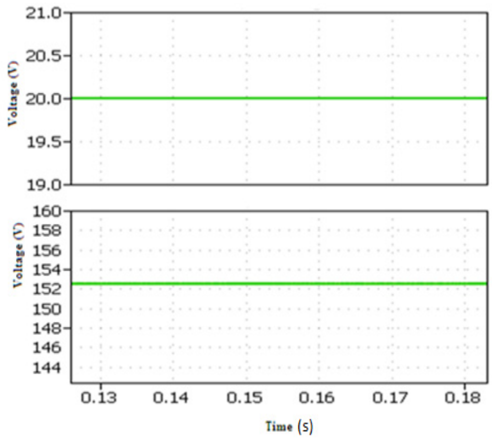

Figure 20. When the input voltage is 20 V, the RVMR output voltage is 153V

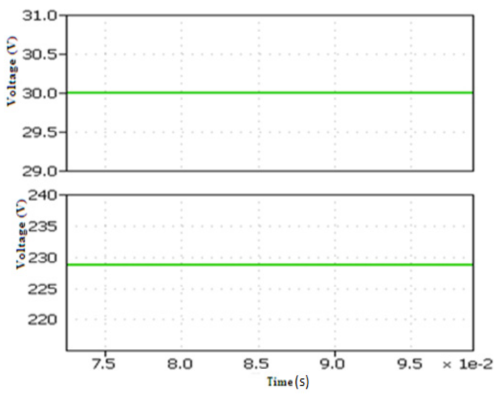

Figure 21. RVMR output voltage 230 V when the input voltage is 30 V

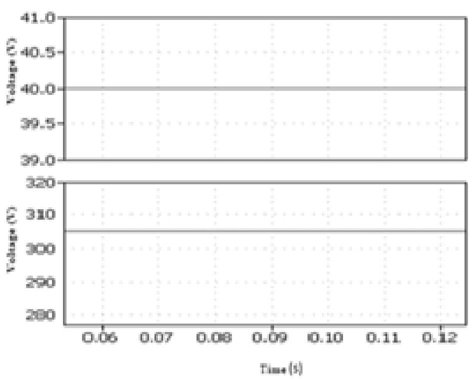

Figure 22. RVMR output voltage when the input voltage is 40 V

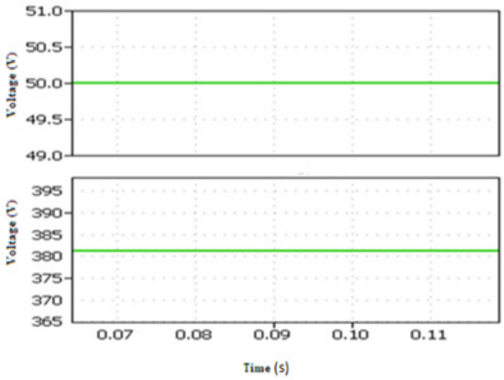

Figure 23. 50 V input voltage produces a 390 V RVMR output voltage

The change of the output voltage concerning the input voltage is shown in Table II and also in Fig. 19-23.

TABLE II. INPUT VOLTAGES AND THE CORRESPONDING BOOST VOLTAGE

Input Voltage (V)	**Boost Voltage (V)**
10	76
20	152
30	228
40	307
50	384

TABLE III. INPUT VOLTAGES AND THE CORRESPONDING CONTROL GAIN (G)

Input Voltage (V)	**Control Gain (G)**
10	7.56
20	7.62
30	7.63
40	7.65
50	7.68

RVMR output voltage is represented in Fig. 24 as a function of input voltage in this diagram. Fig. 25 depicts the relationship between the circuit's gain determined by the input voltage.

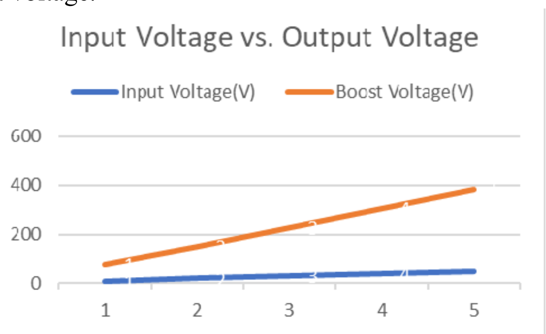

Figure 24. Variation between an input voltage and output voltage

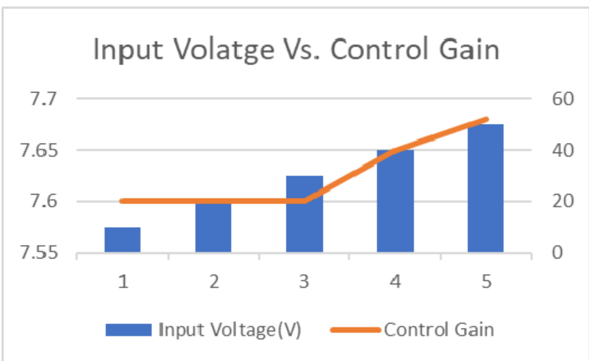

Figure 25. Variations of input voltage and control gain

VIII. CONCLUSION

The photovoltaic network is integrated with the modified RVMR. According to the results of the simulations, the new characteristics of the RVMR ensure a steady rise in voltage and high efficiency. With the proposed RVMR, a high voltage can be increased for a variety of voltage levels by using a connected capacitor and a voltage multiplier in tandem. In real-time applications involving cascading photovoltaic modules, this topology provides the fastest dynamic response and highest voltage amplification. DC-DC amplifier converters will undoubtedly enable more powerful and advanced power converter solutions for state-of-the-art power conversion schemes.

REFERENCES

[1] S. Sathyan, H. M. Suryawanshi, M. S. Ballal, A. B. Shitole, “Soft-switching DC-DC converter for distributed energy sources with high step-up voltage capability,” IEEE Trans. on Ind. Elect., vol. 62, no. 11, pp. 7039-7050, 2015. doi:10.1109/TIE.2015.2448515
[2] R. Teodorescu, M. Liserre, P. Rodriguez, ”Grid converters for photovoltaic and wind power systems,” A John Wiley and Sons, Ltd., 2016. ISBN: 9780470057513
[3] C. Balasundar, S. Sudharshanan, R. Elakkiyavendan, “Design of an optimal tip speed ratio control MPPT algorithm for standalone WECS,” International Journal for Research in Applied Science and Engineering Technology, vol. 3, pp. 54-61, 2015. https://www.ijraset.com/fileserve.php?FID=2435
[4] I. Boldea, “Electric generators and motors: An overview,” CES Transactions on Electrical Machines and Systems, vol. 1, no. 1, pp. 3-14, 2017. doi:10.23919/TEMS.2017.7911104
[5] S. J. Chen, S. P. Yang, C. M. Huang, C. K. Lin, "Interleaved high step-up DC-DC converter with parallel-input series-output configuration and voltage multiplier module," 2017 IEEE International Conference on Industrial Technology (ICIT), 2017, pp. 119-124. doi:10.1109/ICIT.2017.7913069
[6] S. Sun, M. Dong, B. Liang, "Real-time power balancing in electric grids with distributed storage," IEEE Journal of Selected Topics in Signal Processing, vol. 8, no. 6, pp. 1167-1181, Dec. 2014. doi:10.1109/JSTSP.2014.2333499
[7] J. Baek, K. -W. Kim, H. -S. Youn, C. -E. Kim, "High-efficiency LLC resonant converter with reconfigurable voltage multiplying rectifier for wide output voltage applications," IEEE Transactions on Power Electronics, vol. 36, no. 7, pp. 7641-7651, July 2021. doi:10.1109/TPEL.2020.3047005
[8] Z. Hu, L. Wang, Y. Qiu, Y. -F. Liu, P. C. Sen, "An accurate design algorithm for LLC resonant converters - Part II," in IEEE Transactions on Power Electronics, vol. 31, no. 8, pp. 5448-5460, Aug. 2016. doi:10.1109/TPEL.2015.2496179
[9] W. Feng, F. C. Lee, P. Mattavelli, "Optimal trajectory control of burst mode for LLC resonant converter," in IEEE Transactions on Power Electronics, vol. 28, no. 1, pp. 457-466, Jan. 2013. doi:10.1109/TPEL.2012.2200110
[10] U. Nandhalaalaa, S. Ramkumar, M. Muruganandam, “High static gain for solar application using modified SEPIC converter,” International Journal of Innovative Research in Science, Engineering and Technology, vol. 4, pp. 34-41, 2015
[11] H. Wen, D. Jiao, J. -S. Lai, "Light load operation analysis for mhz gan based llc resonant converter," 2020 IEEE 9th International Power Electronics and Motion Control Conference (IPEMC2020-ECCE Asia), 2020, pp. 1087-1090. doi:10.1109/IPEMC-ECCEAsia48364.2020.9368085
[12] N. N. Strain, J. Sun, X. Huang, D. J. Costinett, L. M. Tolbert, "ZVS analysis of a GaN-based series-parallel dual transformer LLC resonant converter," 2019 IEEE 7th Workshop on Wide Bandgap Power Devices and Applications (WiPDA), 2019, pp. 398-404. doi:10.1109/WiPDA46397.2019.8998789
[13] R. Sathishkumar, V. Malathi, E. Sakthivel, “Real-time implementation of quazi Z source inverter incorporated with renewable energy source,” Published in Elsevier Energy Procedia, Vol. 117, pp. 927-934, 2017. doi:10.1016/j.egypro.2017.05.212
[14] R. Sathishkumar, V. Malathi, P. Deepamangai “Quazi Z-source inverter incorporated with hybrid renewable energy sources for microgrid applications,” in Journal of Electrical Engineering, Vol. 16, pp. 458-467, 2017

[15] J. Chen, H. Peng, Y. Kang, J. Wu, X. Chu, "Accurate steady-state modeling and design based on state trajectory analysis for LCC resonant converter with voltage doubler rectifier," IEEE Transactions on Power Electronics, vol. 37, no. 9, pp. 10698-10712, Sept. 2022. doi:10.1109/TPEL.2022.3165591

[16] H. Wu, T. Xia, X. Zhan, P. Xu, Y. Xing, "Resonant converter with resonant-voltage-multiplier rectifier and constant-frequency phase-shift control for isolated buck–boost power conversion," IEEE Transactions on Industrial Electronics, vol. 62, no. 11, pp. 6974-6985, Nov. 2015. doi:10.1109/TIE.2015.2443097

[17] S. K. Changchien, T. J. Liang, J. F. Chen, L.S. Yang, “Step-up DC–DC converter by coupled inductor and voltage-lift technique,” IET Power Electronics, vol. 3, no. 3, pp. 369-378. 2010. doi:10.1049/iet-pel.2009.0089

[18] J. Chen, H. Peng, Y. Kang, J. Wu, X. Chu, "Accurate steady-state modeling and design based on state trajectory analysis for LCC resonant converter with voltage doubler rectifier," IEEE Transactions on Power Electronics, vol. 37, no. 9, pp. 10698-10712, 2022. doi:10.1109/TPEL.2022.3165591

[19] M. Abbasi, R. Emamalipour, M. A. M. Cheema, J. Lam, "A constant-frequency high-voltage gain resonant converter module with semiactive phase-shifted voltage multiplier for MVdc distribution," in IEEE Journal of Emerging and Selected Topics in Power Electronics, vol. 10, no. 4, pp. 3603-3616, Aug. 2022. doi:10.1109/JESTPE.2021.3088120

[20] F. Alaql, A. Alhatlani, I. Batarseh, "Improved LLC resonant converter with rectifier operating in three operation modes for wide voltage range applications," IEEE Applied Power Electronics Conference and Exposition (APEC), 2021, pp. 1945-1950. doi:10.1109/APEC42165.2021.9487319

[21] V. R. Vakacharla, A. K. Rathore, R. K. Singh, S. K. Mishra, "Fixed-frequency current-fed LCL series resonant soft-switching converter with capacitive doubler," in IEEE Transactions on Industry Applications, vol. 57, no. 6, pp. 6611-6621, 2021. doi:10.1109/TIA.2021.3114269

[22] P. Wisutmetheekorn, V. Chunkag, "DSP based control implementation of an AC/DC converter with improved input current distortion," Advances in Electrical and Computer Engineering, vol.11, no.2, pp.87-94, 2011. doi:10.4316/AECE.2011.02014

[23] T. Divya, R. Ramaprabha, "Embedded switched Z-source multilevel inverter for grid interfaced photovoltaic systems," Advances in Electrical and Computer Engineering, vol. 22, no. 3, pp. 43-52, 2022. doi:10.4316/AECE.2022.03005

[24] G. H. Liu, Y. B. Chen, Y. Gao, J. -N. Zhu, B. -X. Wang, T. Yang, "Component-based and machine learning aided optimal filter design for full-bridge current doubler rectifier," IECON 2021 – 47th Annual Conference of the IEEE Industrial Electronics Society, 2021, pp. 1-6. doi:10.1109/IECON48115.2021.9589272

[25] M. R. Ahmed, X. Wei, Y. Li, "Enhanced models for current-mode controllers of the phase-shifted full bridge converter with current doubler rectifier," 10th International Conference on Power Electronics and ECCE Asia (ICPE 2019 - ECCE Asia), 2019, pp. 3271-3278. doi:10.23919/ICPE2019-ECCEAsia42246.2019.8797324

[26] H. P. Paz, V. S. Silva, E. V. V. Cambero, H. X. Araújo, I. R. S. Casella, C. E. Capovilla, “A survey on low power RF rectifiers efficiency for low-cost energy harvesting applications,” AEU - International Journal of Electronics and Communications, Vol. 112, 2019, pp.152963. doi:10.1016/j.aeue.2019.152963